

Fragmentation of CF_4^{q+} ($q = 2, 3$) induced by 1-keV electron collisions

Lei Chen^{①,1}, Enliang Wang^{②,*}, Xu Shan,¹ Zhenjie Shen,¹ Xi Zhao,¹ and Xiangjun Chen^{1,†}

¹Hefei National Laboratory for Physical Sciences at the Microscale and Department of Modern Physics, University of Science and Technology of China, Hefei 230026, China

²J. R. Macdonald Laboratory, Physics Department, Kansas State University, Manhattan, Kansas 66506, USA



(Received 29 March 2021; revised 26 August 2021; accepted 27 August 2021; published 10 September 2021)

We report on an investigation on the fragmentation dynamics of CF_4^{q+} ($q = 2, 3$) induced by 1-keV electron collisions utilizing an ion momentum imaging spectrometer. From the time-of-flight correlation maps five dominating dissociation channels of CF_4^{2+} as well as one three-body fragmentation channel of CF_4^{3+} are identified. The kinetic energy release (KER) distributions for these channels are obtained and compared with the data available in the literature. The Dalitz-like momentum diagram and the Newton diagram are employed to analyze the breakup mechanism in the three-body fragmentation channel. We found that, for CF_4^{2+} dissociation into $\text{F}^+ + \text{CF}_2^+ + \text{F}$, $\text{F}^+ + \text{CF}^+ + 2\text{F}$, and $\text{F}^+ + \text{F}^+ + \text{CF}_2$, the concerted breakup is the dominating process. Channel $\text{C}^+ + \text{F}^+ + 3\text{F}$ is dominated by the initial charge separation, i.e., $\text{CF}_4^{2+} \rightarrow \text{F}^+ + \text{CF}^+ + 2\text{F} \rightarrow \text{C}^+ + \text{F}^+ + 3\text{F}$. With the help of the native frame method, we assigned one sequential pathway and two concerted pathways for channel $\text{CF}_4^{3+} \rightarrow \text{F}^+ + \text{F}^+ + \text{CF}_2^+$. The branching ratios of these pathways are determined. The momentum correlation of the fragments and the deduced KER distribution indicate that different excited states of CF_4^{3+} with different geometries are responsible for these three pathways. The Coulomb explosion model simulation shows that most of the events in this channel are produced by CF_4^{3+} ions that have deformed geometries from the neutral CF_4 molecule.

DOI: [10.1103/PhysRevA.104.032814](https://doi.org/10.1103/PhysRevA.104.032814)

I. INTRODUCTION

The CF_4 molecule has attracted much attention in recent years. It is a super greenhouse gas [1,2] in the earth's atmosphere with a lifetime of about 50 000 years, making it 6500 times more harmful than CO_2 [3]. CF_4 is also a widely used plasma etching gas in the semiconductor industry. The ionic and neutral fragments produced by electron collisions with CF_4 play a vital role in the dry plasma processing of semiconductor materials [4]. Therefore, investigations on fragmentation dynamics of CF_4 are not only of extensive interest in fundamental physics but also of great significance in applications in planet atmospheres and the plasma industry.

In the past few decades, the dissociation of CF_4^{2+} has been intensively studied by electron impact [5–7], photoionization [8–13], and ion collisions [14–16]. Photoion-photoion coincidence (PIPICO), photoelectron-photoion-photoion coincidence (PEPIPICO), and threshold photoelectron-photoion-photoion coincidence (TPEPIPICO) methods have been used to identify the fragmentation pathways, obtaining kinetic energy release (KER) and appearance potentials, as well as analyzing the dissociation mechanisms of the incomplete Coulomb explosion channels. The most frequently investigated channels are $\text{CF}_4^{2+} \rightarrow \text{F}^+ + \text{CF}_3^+$, $\text{CF}_4^{2+} \rightarrow \text{F}^+ + \text{CF}_2^+ + \text{F}$, $\text{CF}_4^{2+} \rightarrow \text{F}^+ + \text{CF}^+ + 2\text{F}$, $\text{CF}_4^{2+} \rightarrow \text{C}^+ + \text{F}^+ + 3\text{F}$, and $\text{CF}_4^{2+} \rightarrow \text{F}^+ + \text{F}^+ + \text{CF}_2$. In these studies, only

time-of-flight (TOF) information of the ionic fragments was obtained rather than imaging their three-dimensional momentum vectors. In the TOF correlation maps, momentum correlations among the fragments result in distinct island shapes for different dissociation mechanisms [17–19]. The shapes of the correlation islands are thus used in the earlier studies to determine the breakup mechanism, i.e., whether it is a concerted dissociation or a sequential fragmentation. Some incomplete three-body sequential and concerted dissociations, however, could generate similar island shapes [19]. In this case, it is difficult to assign the breakup pathway by just analyzing the island shape. For example, in the previous experiments performed by photoionization [8–11,13] and ion collisions [14], the slopes of the correlation islands for channel $\text{F}^+ + \text{CF}_2^+ + \text{F}$ and channel $\text{F}^+ + \text{CF}^+ + 2\text{F}$ were determined to be about -1 in accordance with the theoretical prediction for the deferred charge separation. Meanwhile, the concerted dissociation can also produce neutral fragments sharing very low momentum in which case the slope of coincidence island is also -1 . However, only the deferred charge separation pathway was proposed in these earlier works due to lack of information about the neutral fragment. Therefore, the determination of the three-dimensional momenta of the fragments is necessary to further clarify the dissociation processes in these channels.

On the other hand, although the three-body fragmentation dynamics of triply charged molecular ions such as CO_2^{3+} [20–22], CS_2^{3+} [23], SO_2^{3+} [24], $\text{C}_2\text{H}_2^{3+}$ [25,26], and $\text{CH}_2\text{CCH}_2^{3+}$ [27] has been extensively studied, the dissociation dynamics of the high-symmetry molecules such as

*enliang@phys.ksu.edu

†xjun@ustc.edu.cn

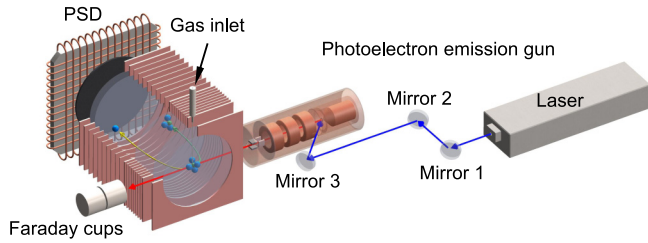


FIG. 1. Schematic diagram of the experimental setup. PSD means position-sensitive detector.

CF_4 and the evidence of geometry deformation of its cation still capture many interests. In its ground states, CF_4 has a tetrahedral structure with T_d symmetry. Previous investigations have demonstrated that the T_d symmetry of CF_4 can be broken in the single [28–33] and double ionization processes [34]. It is reasonable to believe that during the triple ionization process of the CF_4 molecule the fast nuclear motion may also happen leading the produced CF_4^{3+} ion to degenerate from the T_d to lower symmetries. Momentum correlations of three charged fragments will not only be very helpful to analyze the dissociation mechanism but also provide information about the geometry deformation of CF_4^{3+} before the fragmentation.

Recent years have witnessed a great improvement of the position-sensitive detector [35,36] and the coincidence momentum imaging techniques [37,38], making it possible to coincidentally measure the momentum vectors of the ionic fragments and unveil the fragmentation dynamics of small molecules more directly. In the present work, we investigate the fragmentation dynamics of CF_4^{2+} and CF_4^{3+} induced by 1-keV electron impact using an ion momentum imaging spectrometer. With the help of TOF correlation maps, six fragmentation channels are identified. The KER distributions for these channels are obtained and compared with the values available in the literature. By employing the Dalitz-like momentum plot [39], the Newton diagram, and the recently developed native frame method [40], the fragmentation mechanisms of CF_4^{2+} and CF_4^{3+} are investigated.

II. EXPERIMENTAL SETUP AND ANALYSIS PROCEDURE

The experiment was carried out using an ion momentum spectrometer as shown in Fig. 1. Details of the experimental setup have been depicted in Ref. [41]. Briefly, a pulsed electron beam emitted from a photoelectron emission gun collides with the target molecules in the reaction zone. The repetition frequency and pulse duration of the electron pulse are 20 kHz and 0.6 ns, respectively. The spot size of the electron beam is collimated to about 1 mm diameter at the reaction zone. The effusive gas target is introduced into the reaction zone by a copper capillary. After the collision, the projectile is dumped by a set of Faraday cups, while the produced ions are analyzed by a Wiley-McLaren type TOF mass spectrometer [42], followed by a two-dimensional (2D) time- and position-sensitive detector (PSD). The PSD consists of a pair of microchannel plates (MCPs) and a delay line anode (DLA) [35,36]. The TOF of each ion can be deduced by the time difference between its MCP output signal and the laser synchronization

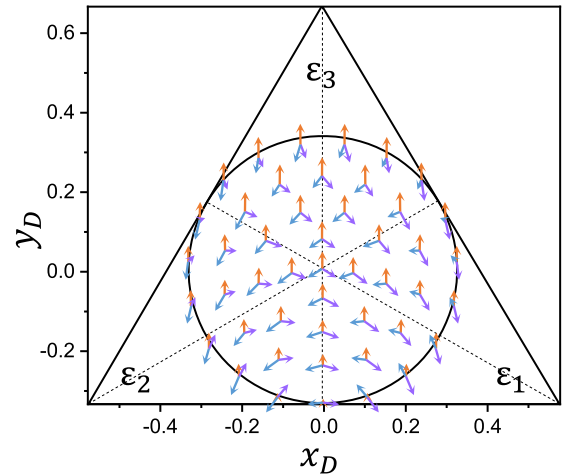


FIG. 2. Definition of the Dalitz-like momentum diagram. The arrows at each point show the momentum correlation of the three fragments.

output signal with a fixed time delay. The impact position on the detector of each ion can be reconstructed with four DLA signals. The three-dimensional momentum vectors of the ion are reconstructed from its TOF and position.

In the experiment, the impinging energy of the electron beam is 1 keV and the average beam current is about 20 pA. The created ions are extracted to the PSD by a pulsed electric field (50 V/cm). The background vacuum of the reaction chamber is better than 1×10^{-6} Pa, and the working pressure is maintained at about 4×10^{-5} Pa to keep a high signal-to-noise ratio.

In this work, we employ the Dalitz plot [39], the Newton diagram, and the native frame method to analyze the three-body breakup processes of CF_4^{q+} ($q = 2, 3$). The Dalitz plot is a powerful analytic tool for visualization of the momentum correlation of the three-body processes. Normally, the Dalitz plot is defined by the normalized kinetic energy of the associating ions. For some channels, the Dalitz plot has different edge shapes due to the different mass of the final species. Here, we use the Dalitz-like momentum diagram which is defined within a regular triangle and the perpendicular distances to the edges of a certain point are defined by the normalized coordinates,

$$\varepsilon_i = \frac{|\mathbf{P}_i|^2}{\sum |\mathbf{P}_j|^2}, \quad (1)$$

where \mathbf{P}_i and \mathbf{P}_j are the momentum vectors of the i th and j th fragments ($i, j = 1, 2, 3$), and the Cartesian coordinates x_D and y_D of the Dalitz-like momentum diagram are defined as

$$x_D = \frac{\varepsilon_1 - \varepsilon_2}{\sqrt{3}}, \quad (2)$$

$$y_D = \varepsilon_3 - \frac{1}{3}. \quad (3)$$

As shown in Fig. 2, each point in the diagram represents a specific momentum correlation pattern of the three fragments. Usually, the localized experimental events in the Dalitz-like

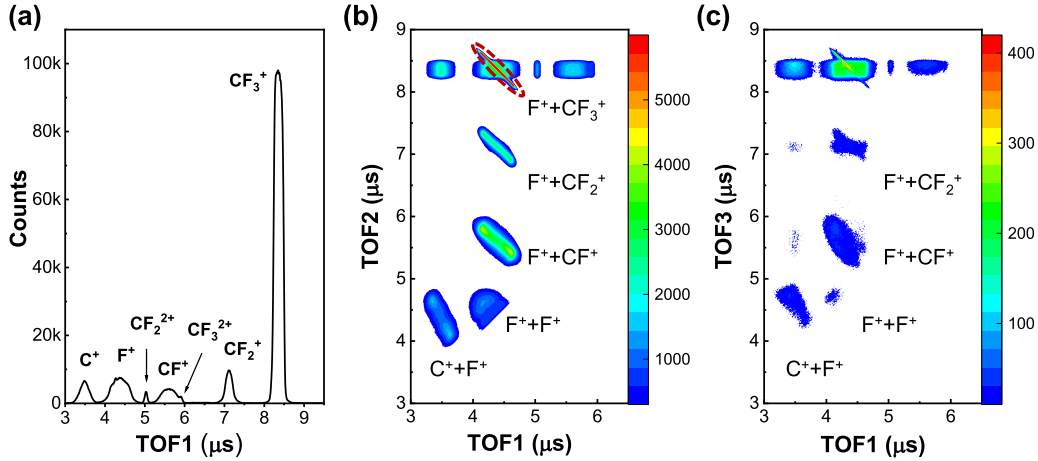


FIG. 3. (a) TOF spectrum of CF_4 produced by 1-keV electron impact; (b) TOF correlation map of the first hit ions vs the second ions; (c) TOF correlation map of the first hit ions vs the third ions. The red dashed oval in (b) is used to select the events of channel $\text{F}^+ + \text{CF}_3^+$.

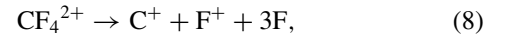
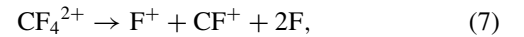
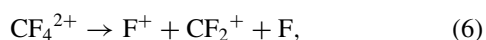
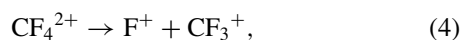
diagram correspond to the concerted fragmentation while the delocalized events scattering along a certain curve originate from the sequential fragmentation [20]. We also use the Newton diagram to have a more straightforward visualization of the momentum correlation of the fragments. In the Newton diagram, the normalized momenta of the three fragments are plotted on a 2D plane with one of them fixed on the x axis and the other two on the upper and lower halves of the plane. The native frame method [40] enables the clear separation of the sequential and concerted breakup by analyzing the three-body fragmentation in the native frame associated with each step and taking advantage of the rotation of the intermediate molecular fragment before its final dissociation. Additionally, this method allows the determination of the branching ratios of these fragmentation processes.

III. RESULTS AND DISCUSSION

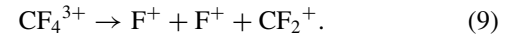
A. TOF spectrum and TOF correlation maps

The TOF spectrum of the fragment ions produced in the collision of a 1-keV electron beam with a CF_4 molecule is shown in Fig. 3(a). The TOF peaks of C^+ , F^+ , CF_2^{2+} , CF^+ , CF_3^{2+} , CF_2^+ , and CF_3^+ can be observed with a high signal-to-noise ratio. The parent ion CF_4^+ , whose TOF peak is expected to be around 9450 ns, is not observed in the present experiment mainly because the involved cationic states, e.g., X^2T_1 , A^2T_2 , and B^2E , of CF_4^+ dissociate into $\text{CF}_3^+ + \text{F}$ within a few femtoseconds [33,43,44]. Figures 3(b) and 3(c) show the TOF correlation map between the first two fragment ions and that between the first and third fragment ions, respectively. For a certain dissociative channel, the true events will distribute along an island on the coincidence map due to the momentum correlation. The following six dominating channels are identified:

Fragmentation channels of CF_4^{2+} ,



and fragmentation channels of CF_4^{3+} ,



It is worth noting that channels (4) and (9) are complete Coulomb explosion channels, while channels (5)–(8) are incomplete Coulomb explosion channels with a neutral fragment in their final outcomes. In principle, the undetected species in channels (5)–(8) could be ions that are lost due to the detection efficiency not being 100%. This situation, however, can be ignored because the ionization cross section decreases heavily with the increasing number of ionized electrons. In the present work, the event counts of fragmentation channels produced by CF_4^{2+} [channel (4)–(8)] are about 6000 times higher than that by CF_4^{3+} [channel (9)]. Even if we take the detection efficiency ($\sim 60\%$) of the third fragment ion into account, the cross section of creating CF_4^{3+} is still three orders lower than that of CF_4^{2+} . Therefore, it is reasonable to assume the undetected fragment to be a neutral particle. For the channels [channel (7) and (8)] with more than one neutral fragment, we regard them as one group and its sum momentum is reconstructed by the momentum conservation. In Figs. 3(b) and 3(c), there are several intense islands produced by false coincidence of the fragment ions, such as $\text{C}^+ + \text{CF}_3^+$, and $\text{CF}^+ + \text{CF}_3^+$. In this work, these islands are not analyzed. For a channel such as $\text{F}^+ + \text{CF}_3^+$, the background behind the true coincidence is not negligible from the TOF correlation map. The background is further filtered by the momentum conservation condition.

B. Fragmentation of CF_4^{2+}

Codling *et al.* [9] determined the appearance potentials for the fragmentation of CF_4^{2+} and tentatively correlated these potentials with two-hole states of CF_4 calculated by Larkins and Tulea [45]. Bruce *et al.* [5] reported the appearance potentials for double-ion formation from the electron impact

TABLE I. Appearance potentials for various dissociation channels of CF_4^{2+} studied in this work.

Channel	Possible two-hole state	Experimental ionization potential (eV)			Calculated double appearance potential (eV)	
		Codling <i>et al.</i> [9]	Bruce <i>et al.</i> [5]	Feifel <i>et al.</i> [12]	Griffiths <i>et al.</i> [46]	Gottfried <i>et al.</i> [47]
$\text{F}^+ + \text{CF}_3^+$	$[1t_14t_2]^3T_1$	37.6 ± 0.6	36	37.2	39.13	38.4211
$\text{F}^+ + \text{CF}_2^+ + \text{F}$	$[4t_24t_2]^3T_1$	42.4 ± 0.7	40	40.7	41.71	41.8540
$\text{F}^+ + \text{CF}^+ + 2\text{F}$	$[4t_24a_1]^3T_2$	47.5 ± 0.9	42	45.1	47.05	47.4319
$\text{C}^+ + \text{F}^+ + 3\text{F}$	$[4t_12t_2]^3E$	62.0 ± 1.5	63			

dissociative ionization of CF_4 . Feifel *et al.* [12] obtained fragmentation pathway-selected double ionization electron spectra of CF_4 by using the TOF PEPECO spectroscopy technique. Griffiths *et al.* [46] measured the Auger-electron spectra of CF_4 and assigned some of the peaks to the population of the electronic states of CF_4^{2+} by using theoretically calculated spectra. A recent calculation was performed by Gottfried *et al.* [47], who derived double ionization potentials of CF_4 with the Green's function method. We list the available experimental and theoretical energy values of CF_4^{2+} in Table I and plot the values given by Codling *et al.* [9] in Fig. 4 to help to understand the present results.

I. Complete fragmentation channel of CF_4^{2+}

The red solid dots in Fig. 5 demonstrate the KER distribution for channel $\text{CF}_4^{2+} \rightarrow \text{F}^+ + \text{CF}_3^+$ which ranges from 2.0 to 10.0 eV with a single peak at about 5.4 eV. The KER peak values in the present experiment and other works are summarized in Table II for comparison. The uncertainties of the present KER peak values are determined by the momentum resolution of the spectrometer and the data statistics. It is worth noting that in the previously reported results the contribution of the neutral atoms to the KER value is not included.

Curtis and Eland [8] obtained a KER value of 5.0 ± 0.2 eV using a helium resonance lamp and the PIPICO technique.

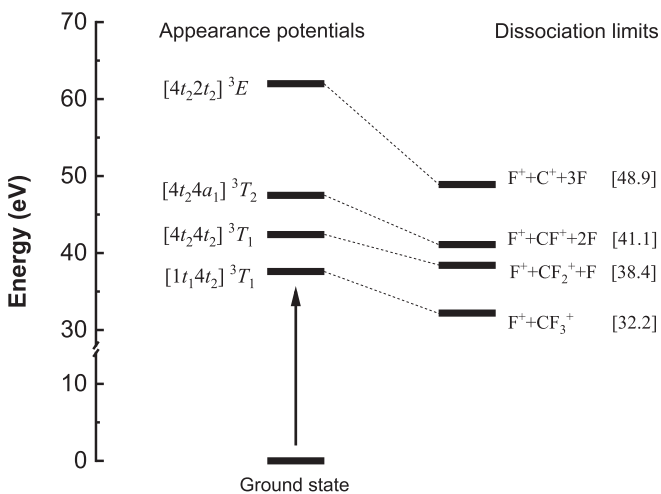


FIG. 4. Schematic diagram illustrating the threshold energies and dissociation limits of CF_4^{2+} . Appearance potentials are adopted from the results of Codling *et al.* [9]. Dissociation limits are derived by using thermochemical data from Rosenstock *et al.* [48].

In the double photoionization experiments, Codling *et al.* [9] also reported a value of 5.0 ± 0.2 eV at 275 Å wavelength and a value of 3.9 ± 0.3 eV at 250 Å wavelength for this channel. They suggested that $[1t_14t_2]^3T_1$ of CF_4^{2+} is responsible for the KER value at 5.0 eV and the CF_3^+ ion and F^+ ion are produced in their ground electronic states. In the soft x-ray absorption experiments, Saito *et al.* [10] derived KER distributions extending from 1 to 10 eV from their selective PIPICO spectra. They measured a KER peak around 4.5 eV below the C K edge and a peak value at about 5.5 eV above the F K edge. The present KER profile agrees well with that of Saito *et al.* obtained above the F K edge. They proposed that the valence double ionization yielded by Auger transitions from the C $1s^{-1}$ hole state and F $1s^{-1}$ hole state are probably responsible for the lower KER value at 4.5 eV and the higher one at 5.5 eV [10], respectively, whereas Thomas *et al.* [11] determined a KER value of 8.7 eV at the C K edge and a value of 8.2 eV at the F K edge from their TPEPIPICO contour maps, which are much higher than the value of the present experiment and other works. Probably, this issue is due to the photoelectron-photoion coincidence in the work of Thomas *et al.* where the electron analyzer can be regarded as a filter to preselect the ionization states. In the experiment of electron transfer collisions between 8.0-keV Ar^{8+} and CF_4 , Motohashi

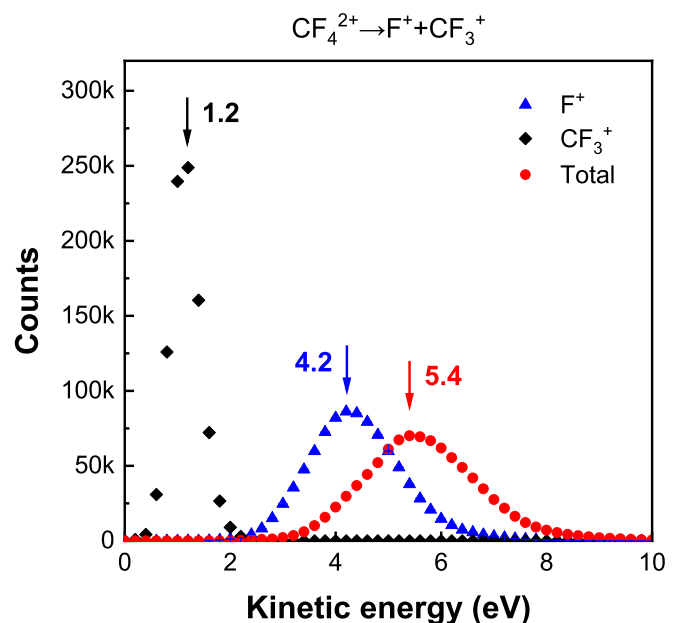


FIG. 5. Kinetic energy distributions for channel $\text{CF}_4^{2+} \rightarrow \text{F}^+ + \text{CF}_3^+$.

TABLE II. KER peak values for fragmentation of CF_4^{q+} ($q = 2, 3$).

Channel	Electron impact This work	Photoionization				Ion collisions Motohashi and Tsurubuchi [14]
		Curtis and Eland [8]	Codling <i>et al.</i> [9]	Saito <i>et al.</i> [10]	Thomas <i>et al.</i> [11]	
$\text{F}^+ + \text{CF}_3^+$	5.4 ± 0.1	5.0 ± 0.2	$3.9 \pm 0.3^{\text{a}}$ $5.0 \pm 0.2^{\text{e}}$	$4.5 \pm 0.5^{\text{b}}$ $5.5 \pm 0.5^{\text{f}}$	8.2^{c} 8.7^{g}	$3.25 \pm 0.06^{\text{d}}$ $3.47 \pm 0.06^{\text{h}}$
$\text{F}^+ + \text{F}^+ + \text{CF}_2$	15.2 ± 0.1			5.0 ± 0.5	$10.7^{\text{c,g}}$	
$\text{F}^+ + \text{CF}_2^+ + \text{F}$	5.4 ± 0.1	3.8 ± 0.2	$3.0 \pm 0.3^{\text{e}}$ $4.7 \pm 0.5^{\text{i}}$	3.8 ± 0.5	7.0^{c} 7.8^{g}	$2.60 \pm 0.04^{\text{d}}$ $2.62 \pm 0.07^{\text{h}}$
$\text{F}^+ + \text{CF}^+ + 2\text{F}$	6.8 ± 0.1	4.1 ± 0.3	$2.8 \pm 0.3^{\text{a}}$ $5.5 \pm 0.6^{\text{i}}$	4.5 ± 0.5	7.7^{c} 8.3^{g}	$3.23 \pm 0.07^{\text{d}}$ $3.04 \pm 0.10^{\text{h}}$
$\text{C}^+ + \text{F}^+ + 3\text{F}$	11.2 ± 0.1		15^{i}	9.0 ± 0.5	12.4^{c} 21.8^{g}	$5.2 \pm 0.13^{\text{h}}$
$\text{F}^+ + \text{F}^+ + \text{CF}_2^+$	17.4 ± 0.5					

^aAt 250 Å wavelength.

^bBelow the C K edge.

^cAt F K edge.

^dDouble-electron transfer.

^eAt 275 Å wavelength.

^fAbove the F K edge.

^gAt C K edge.

^hSingle-electron transfer.

ⁱAt 150 Å wavelength.

and Tsurubuchi [14] estimated a peak value of 3.47 ± 0.06 eV for single-electron transfer and a value of 3.25 ± 0.08 eV for double-electron transfer from their TPEPIPICO maps. As listed in Table II, the present KER distribution peak value at 5.4 eV is in accordance with the results of Codling *et al.* [9] and Saito *et al.* [10], as well as that of Curtis and Eland [8]. We conclude that this peak value comes from the fragmentation of the $[1t_14t_2]$ 3T_1 state of CF_4^{2+} into the ground states of $\text{F}^+ + \text{CF}_3^+$, while the lower values reported by Codling *et al.* [9] (3.9 ± 0.3 eV) at 250 Å wavelength, Saito *et al.* [10] (4.5 ± 0.5 eV) below the C K edge, and Motohashi and Tsurubuchi [14] (3.25 ± 0.06 eV and 3.47 ± 0.06 eV) may originate from lower excited states. In addition to the main contributing states, there are plenty of excited states around the main states [46,47]. For example, the theoretical calculation of Griffiths *et al.* [46] showed that the double ionization band including the $[1t_14t_2]$ 3T_1 state results in a broad binding energy peak with more than 10 eV width. We conclude that, in addition to the main state of $[1t_14t_2]$ 3T_1 , the broad KER distribution in the present work is contributed from various electronic states.

2. Incomplete fragmentation channels of CF_4^{2+}

Identified from the TOF correlation map in Fig. 3(b), four incomplete Coulomb fragmentation channels of CF_4^{2+} are observed, i.e., $\text{CF}_4^{2+} \rightarrow \text{F}^+ + \text{F}^+ + \text{CF}_2$, $\text{CF}_4^{2+} \rightarrow \text{F}^+ + \text{CF}_2^+ + \text{F}$, $\text{CF}_4^{2+} \rightarrow \text{F}^+ + \text{CF}^+ + 2\text{F}$, and $\text{CF}_4^{2+} \rightarrow \text{F}^+ + \text{C}^+ + 3\text{F}$. In the following analysis, the undetected neutral components are regarded as one group and its momentum is reconstructed by the momentum conservation. Figure 6 shows the Dalitz-like momentum diagrams, the Newton diagrams, and kinetic energy distributions for the first three channels.

Channel $\text{F}^+ + \text{F}^+ + \text{CF}_2$. The fragmentation mechanism of channel $\text{CF}_4^{2+} \rightarrow \text{F}^+ + \text{F}^+ + \text{CF}_2$ cannot be determined simply from the shape and slope of the island in Fig. 3(b) due to the very broad distribution. The Dalitz-like momentum diagram for this channel is exhibited in Fig. 6(a) where the highest-density point is located around (0, 0.06) indicating that the momentum magnitudes of two F^+ ions are almost identical, and the neutral fragment group (CF_2) shares considerable recoil momentum. Figure 6(b) demonstrates the Newton diagram with the CF_2 group fixed on the x axis and these two F^+ ions plotted on the lower and upper half planes. In this diagram, the momenta of these two F^+ ions distribute symmetrically respective to the x axis and the most probable momentum correlation angles between the two F^+ ions and the CF_2 group are both 124° . These features indicate that this fragmentation channel undergoes a concerted breakup process, where two F-C bonds break simultaneously once the CF_4 molecule is doubly ionized. As the F-C bonds stretch, the CF_2 group obtains considerable recoil momentum due to the triangle geometry of $\text{F}^+ - \text{C} - \text{F}^+$. Thomas *et al.* [11] have reported a similar fragmentation mechanism in their soft x-ray core shell ionization experiment. Figure 6(c) shows the KER distribution for this channel, which extends from 3 to about 35 eV with a peak at 15.2 eV. To compare with the total kinetic energy distributions of previously published results, we plot the sum kinetic energy of $\text{F}^+ + \text{F}^+$. As shown by the purple curves in Fig. 6(c), the sum kinetic energy ranges from 1 to 30 eV which is broader than the distribution obtained by Saito *et al.* [10]. The peak value of KER determined in this work (15.2 eV) is much higher than that given by Saito *et al.* [10] (5.0 eV); however, it is in reasonable agreement with that of Thomas *et al.* [11] (10.7 eV). The reasons for the low value of Saito *et al.* are mainly due to their assumption that the

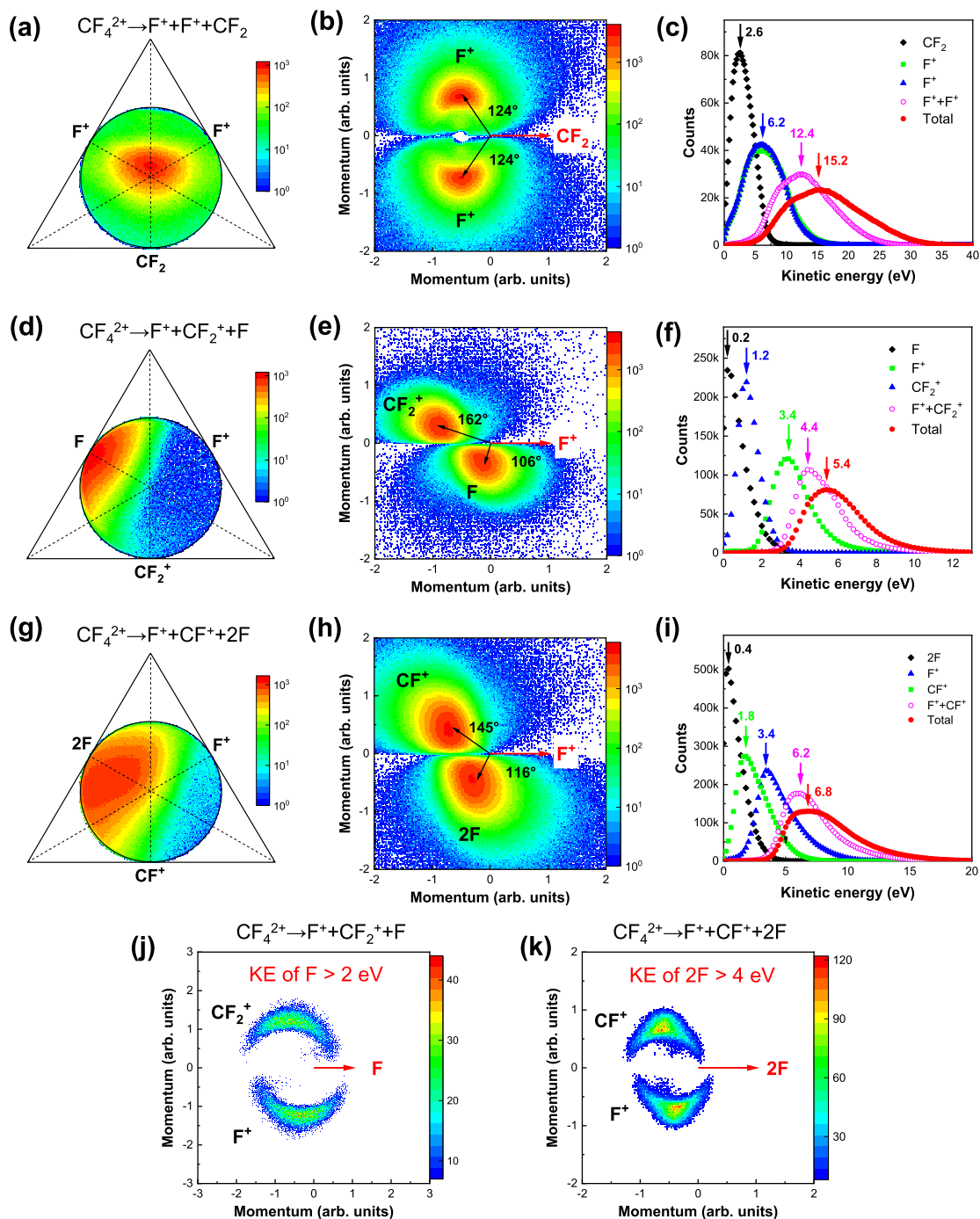


FIG. 6. Dalitz-like momentum diagrams, Newton diagrams, and kinetic energy (KE) distributions for incomplete Coulomb fragmentation of CF_4^{2+} : (a)–(c), channel $\text{CF}_4^{2+} \rightarrow \text{F}^+ + \text{F}^+ + \text{CF}_2$; (d), (e) channel $\text{CF}_4^{2+} \rightarrow \text{F}^+ + \text{CF}_2^+ + \text{F}$; (g)–(i) $\text{CF}_4^{2+} \rightarrow \text{F}^+ + \text{CF}^+ + 2\text{F}$; (j), (k) Newton plots filtered by kinetic energy of the neutral fragment(s).

neutral CF_2 group has no kinetic energy and the two F^+ ions are emitted back to back.

Channel $\text{F}^+ + \text{CF}_2^+ + \text{F}$. For channel $\text{CF}_4^{2+} \rightarrow \text{F}^+ + \text{CF}_2^+ + \text{F}$, an island of about -1 is deduced from Fig. 3(b) which agrees with the theoretical value for the sequential fragmentation process, i.e., $\text{CF}_4^{2+} \rightarrow \text{CF}_3^{2+} + \text{F} \rightarrow \text{F}^+ + \text{CF}_2^+ + \text{F}$. This sequential pathway has been reported in several earlier works [9–11,14,17]. However, we still cannot exclude the possibility of the concerted fragmentation

where the neutral F atom receives very low momentum, which also results in a bar-shaped island of slope -1 . Figure 6(d) shows the experimental Dalitz-like momentum diagram for this channel. In this plot, an intense area near the edge of the F axis is observed indicating that the momenta of most neutral F atoms are around zero. In Fig. 6(e), the Newton diagram for this channel is shown with the normalized momentum of the F^+ ion fixed at the x axis while the F atom and the CF_2^+ ion are plotted on the lower and upper half plane. Clearly, the

most intense area corresponds to the concerted mechanism where the F atom shares small momentum. In this diagram, the peak of the correlation angle between the F^+ ion and the CF_2^+ ion is 162° , suggesting that these two fragment ions are emitted almost back to back, leaving the neutral F atom almost at rest. These features are strong evidence of the concerted breakup. On the other hand, as discussed in the following, the sequential fragmentation via $F + CF_3^{2+}$ to $F^+ + CF_2^+ + F$ cannot be ignored. As shown in Fig. 6(f), the kinetic energy of the F atom distributes from 0 to 4 eV with a peak of around 0.2 eV. Reading from the Newton diagram, i.e., Fig. 6(e), the high-energy (large momentum) F atoms are very likely produced through sequential fragmentation. In order to examine whether this neutral F atom is emitted in the first step of the sequential breakup process, we draw another Newton diagram where all the momenta of the fragments are normalized to the magnitude of the neutral F atom. As shown in Fig. 6(j), the Newton diagram is filtered by the kinetic energy of the F atom. The circular structure is strong evidence of the sequential fragmentation process. Interestingly, close to the bottom line of the CF_2^+ axis in the Dalitz-like diagram of Fig. 6(d), an area with enhanced density is observed. These events correspond to the sequential fragmentation with the F atom emitted with rather high momentum. Figure 6(f) shows the KER distribution for channel $CF_4^{2+} \rightarrow F^+ + CF_2^+ + F$ which disperses from 3 to 12 eV with a peak at 5.4 eV. The KER peak value in the present work is in good agreement with that obtained by Codling *et al.* at a photon wavelength of 150 Å (5.5 ± 0.5 eV) [9], and lower than the values of Thomas *et al.* (7.8, 7.0 eV) [11], and higher than the values of Motohashi and Tsurubuchi (2.62, 2.60 eV) [14] and Codling *et al.* (3.8 ± 0.5 eV at 275 Å) [9]. It is worth noting that, in the studies of Motohashi and Tsurubuchi [14] and Thomas *et al.* [11], the energy of the neutral F atom is not included in the KER while Codling *et al.* [9] assigned a kinetic energy value of 0.8 eV to the F atom. The present sum kinetic energy distribution for $C^+ + CF_2^+$ extends from 2 to 12 eV with a peak at 4.4 eV which is very similar to that reported by Saito *et al.* [10] who derived a sum kinetic energy distribution (peak at 3.8 ± 0.5 eV) for the $C^+ + CF_2^+$ from their PEPICO spectrum by assuming a two-step fragmentation scheme ($CF_4^{2+} \rightarrow CF_3^{2+} + F \rightarrow F^+ + CF_2^+ + F$). Codling *et al.* [9] proposed that the two-hole state $[4t_24t_2] {}^3T_1$ may be responsible for the KER value at 3.8 eV and suggested that the sequential fragmentation is possible at 275 Å wavelength. Therefore, we conclude that the present KER peak value at 5.4 eV is very likely the contribution from a higher excited state of CF_4^{2+} , which prefers to dissociate into $F^+ + CF_2^+ + F$.

Channel $F^+ + CF^+ + 2F$. Channel $CF_4^{2+} \rightarrow F^+ + CF^+ + 2F$ has four fragments in its final states, in which the two neutral atoms cannot be detected, making it difficult to analyze the fragmentation mechanism. In Fig. 3(b), we determine an island slope of about -1 for this channel which agrees with the theoretically predicted value for the sequential breakup ($CF_4^{2+} \rightarrow CF_2^{2+} + 2F \rightarrow F^+ + CF^+ + 2F$). Both Codling *et al.* [9] and Thomas *et al.* [11] have suggested a similar fragmentation mechanism for this channel. However, as discussed above, a concerted dissociation with the neutral F atoms sharing very low momentum can also generate an island slope of -1 . By regarding two F atoms as one

group and applying the momentum conservation law, we obtained the momentum of the group (2F). In Fig. 6(g), the Dalitz-like momentum diagram for this channel is displayed. Like the case of channel $CF_4^{2+} \rightarrow F^+ + CF_2^+ + F$, most of the events in this plot are scattering closely to the 2F axis, indicating that the neutral 2F group shares very limited momentum. In the Newton diagram for this channel [see Fig. 6(h)], two high-density areas can be observed. The most probable angle between the CF^+ ion and the F^+ ion is 145° indicating that these two ionic fragments fly almost back to back. The deviation from 180° is caused by the recoil of the neutral group (2F). As shown in Fig. 6(i), the kinetic energy of the neutral group (2F) has a wide distribution from 0 to 5 eV with a sharp peak at 0.4 eV. We propose that this channel is also dominated by the fast concerted breakup. In this channel, the undetected neutral atoms induce more uncertainties where other dissociation processes may be also involved; e.g., the isomerization process may happen during the dissociation which results in channel $CF_4^{2+} \rightarrow CF_2^{2+} + F_2$. On the other hand, as discussed in the following, the sequential fragmentation mechanism cannot be ignored. Figure 6(k) shows the Newton diagram drawn by selecting the high-energy 2F groups (kinetic energy higher than 4 eV). The circular structure in this diagram suggests that these high-energy 2F groups are produced by the sequential breakup, e.g., $CF_4^{2+} \rightarrow CF_2^{2+} + 2F \rightarrow F^+ + CF^+ + 2F$. In Fig. 6(i), the KER distribution for this channel exhibits a broad peak of around 6.8 eV. This value is in good agreement with that obtained by Codling *et al.* (6.3 ± 0.6 eV) in the 150 Å wavelength photon double ionization experiment [9]. The present sum kinetic energy distribution of $F^+ + CF^+$ ranges from 3 to 15 eV which is much broader than that given by Saito *et al.* [10], and the peak value (6.2 eV) determined in this work is higher than the value (4.5 eV) of Saito *et al.* Codling *et al.* [9] suggested that the $[4t_24a_1] {}^3T_2$ state of CF_4^{2+} is responsible for this channel.

Channel $C^+ + F^+ + 3F$. As shown in Fig. 3(b), the angle of island $C^+ + F^+$ with respect to the x axis is determined to be about 63° . This value is the same as that reported by Bruce *et al.* [7] at an electron impact energy of 100 eV. However, as their electron impact energy increased from 100 to 500 eV, the angle is increased monotonically to 69° . Codling *et al.* [9] and Thomas *et al.* [11] also observed an angle of 69° in their photoionization experiments which was in good accordance with the value predicted by the theory [19] for the sequential fragmentation with initial charge separation $CF_4^{2+} \rightarrow F^+ + CF^+ + 2F \rightarrow C^+ + F^+ + 3F$, where the first step is a fast concerted breakup emitting two low-energy F atoms, while the second step is much slower. Motohashi and Tsurubuchi [14] measured an angle of 57° in the Ar^{8+} and CF_4 collisions and proposed a direct fragmentation mechanism for this channel, i.e., $CF_4^{2+} \rightarrow C^+ + F^+ + 3F$. In the present work, the obtained angle (63°) is larger than that expected for the deferred charge separation (45°) or the fast concerted dissociation with the neutral fragments sharing very low momentum (45°), but smaller than that for a sequential fragmentation with initial charge separation (69°). Considering there are three undetected neutral F atoms in this channel which induce more uncertainties, all these dissociation processes may be involved in this channel among which the initial charge separation is

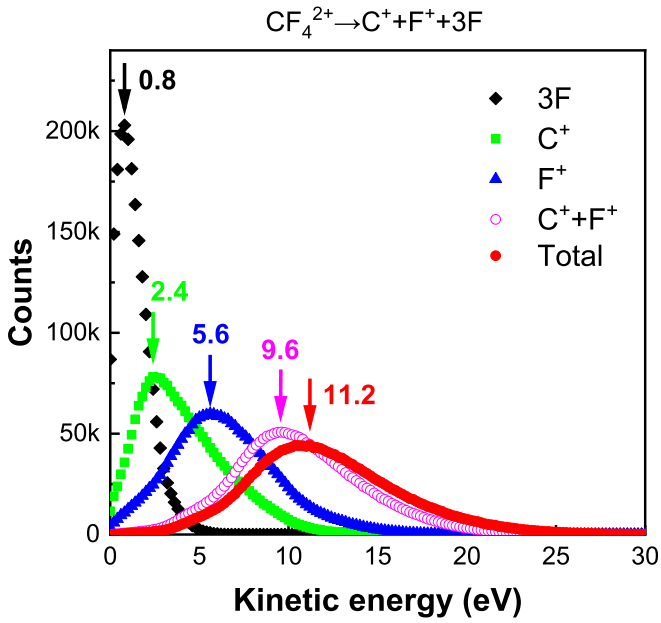


FIG. 7. Kinetic energy distributions for channel $\text{CF}_4^{2+} \rightarrow \text{C}^+ + \text{F}^+ + 3\text{F}$.

the dominant one. By assuming the neutral fragments as one group, we obtained the kinetic energy distributions for this channel. As shown in Fig. 7, the KER distribution ranges from 3 to about 25 eV with a peak around 11.2 eV. The present sum kinetic energy distribution for $\text{C}^+ + \text{F}^+$ ranges from 0 to 25 eV with a peak value at 9.6 eV agreeing well with that reported by Saito *et al.* [10] (peak value at 9.0 ± 0.5 eV). The peak value of this work and that of Saito *et al.* are lower than the result of Codling *et al.* [9] who assigned $[4t_22t_2]$ 3E for the KER value at ~ 15 eV.

C. Three-body fragmentation of CF_4^{3+}

From the TOF correlation maps in Figs. 3(b) and 3(c), a complete three-body Coulomb fragmentation channel of CF_4^{3+} is identified, i.e., channel $\text{CF}_4^{3+} \rightarrow \text{F}^+ + \text{F}^+ + \text{CF}_2^+$, which can be extracted by $\text{F}^+ + \text{F}^+$ and $\text{F}^+ + \text{CF}_2^+$ co-

incidence by the first vs second hit and first vs third hit ions, respectively. Triple coincidence events are first selected by the momentum conservation and further filtered by the momentum-energy correlation spectrum to reduce accidental coincidence [49]. As shown in Fig. 8(a), the obtained Dalitz-like momentum diagram demonstrates a V-shape structure. According to the momentum vector correlation, these two wings originate from sequential dissociation of CF_4^{3+} into $\text{F}^+ + \text{F}^+ + \text{CF}_2^+$ via $\text{F}^+ + \text{CF}_3^{2+}$, while events in the high-density areas come from concerted breakup processes. The Newton diagram for this channel is present in Fig. 8(b) where the momentum vector of the F_a^+ ion (F^+ ion with higher momentum value) is fixed on the x axis and the other F^+ ion (F_b^+) and the CF_2^+ ion are plotted on the lower and upper half planes of the diagram. The momentum magnitude of the F_a^+ ion is used to normalize the momentum magnitudes of all three fragment ions. The circular structure indicates the existence of a rotation process between F_b^+ and CF_2^+ which is a clear sign of a sequential fragmentation process $\text{CF}_4^{3+} \rightarrow \text{F}_a^+ + \text{CF}_3^{2+} \rightarrow \text{F}_a^+ + \text{F}_b^+ + \text{CF}_2^+$.

Here, we introduce the native frame method [40] to further analyze the sequential and concerted mechanism. Assuming sequential breakup of CF_4^{3+} via $\text{F}_a^+ + \text{CF}_3^{2+}$, a density graph of the events in this channel is plotted by the angle (θ) vs energy (KER of CF_3^{2+}). θ is defined by the relative angle between the momentum vector of F_a^+ and CF_3^{2+} in the native frame, where the former one is defined by the relative momentum of F_a^+ with respect to the center of mass of the CF_3^{2+} and the latter one is defined by the relative momentum between F_b^+ and CF_2^+ . The KER of CF_3^{2+} is defined as the kinetic energy released in the second step. The sequential fragmentation will form a uniform angular distribution which has no correlation with the kinetic energy distribution while a strong correlation will be presented in the concerted mechanism. Figure 8(c) shows the native frame plot. The uniform angular distribution along $\text{KER} \sim 4.0$ eV further verifies the existence of the sequential breakup through an intermediate state of CF_3^{2+} , while the events localized around $\theta \sim 90^\circ$ are mainly produced by concerted breakup processes.

To have a deeper understanding of the involved fragmentation processes, we filter these plots by windows A–C. As

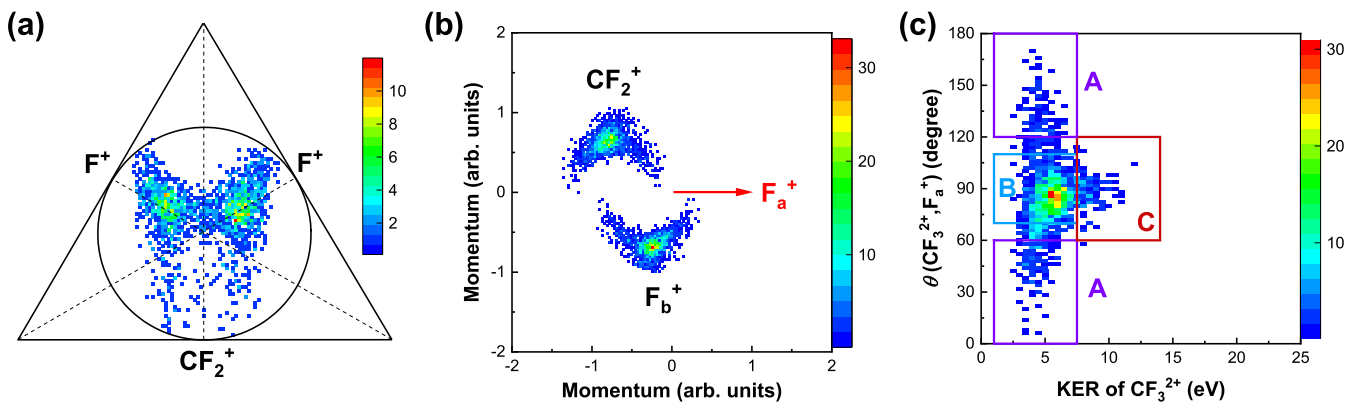


FIG. 8. Channel $\text{CF}_4^{3+} \rightarrow \text{F}^+ + \text{F}^+ + \text{CF}_2^+$: (a) Dalitz-like momentum diagram, (b) Newton diagram, and (c) KER of CF_3^{2+} vs θ (CF_3^{2+} , F_a^+) native frame plot by assuming sequential breakup of CF_4^{3+} via $\text{F}_a^+ + \text{CF}_3^{2+}$. F_a^+ and F_b^+ are the F^+ ions with higher and lower kinetic energy, respectively.

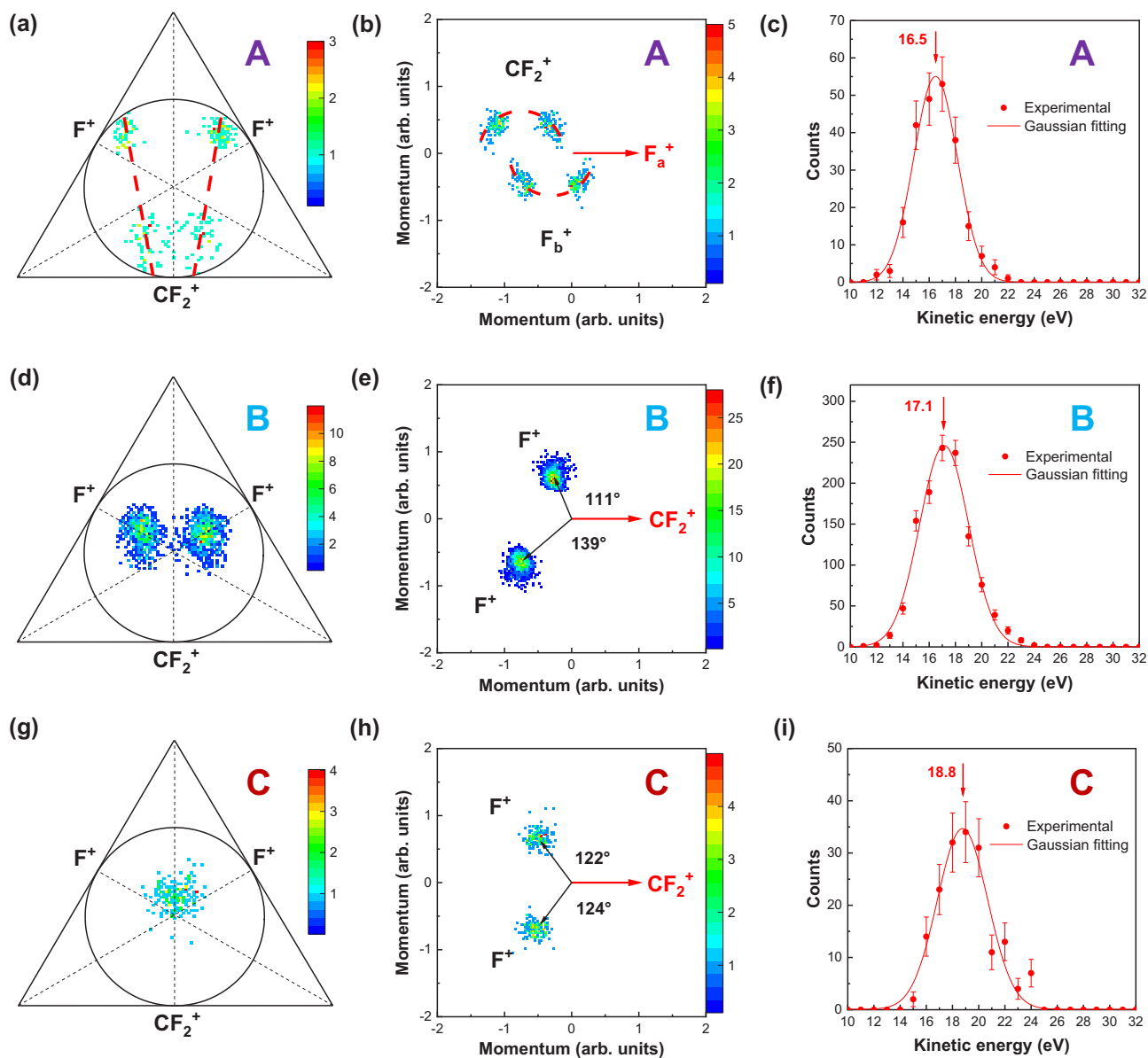


FIG. 9. Dalitz-like momentum diagrams, Newton diagrams, and KER distributions for regions A–C in Fig. 8(c).

discussed above, events in region A come from sequential fragmentation while those in regions B and C are from two different concerted breakup processes. Figure 9 displays the Dalitz-like momentum diagrams, Newton diagrams, and KER distributions for these three regions. The Dalitz-like momentum diagram in Fig. 9(a) and the Newton diagram in Fig. 9(b) further confirm that the events in region A originate from a sequential fragmentation. In Fig. 9(d), the Dalitz-like momentum diagram for region B shows two high-density spots and the Newton diagram for this region shows two intense islands, which is a typical characteristic of the concerted breakup. For the Newton diagram of the concerted mechanism, the F^+ with lower and higher energies are plotted on the upper and lower half planes. The most probable correlation angle between the momentum vector of CF_2^+ and the higher-energy F^+ ion is 139° , larger than that between CF_2^+ and the lower-energy one (111°). In Fig. 9(g), events in the Dalitz-like momentum

diagram for region C distribute near the origin where the momentum magnitudes of two F^+ ions are almost identical, and both are a little bit smaller than that of CF_2^+ . This situation can only occur in a concerted breakup. The Newton diagram in Fig. 9(h) demonstrates the momentum correlation of these three fragment ions more directly where the momenta of the two F^+ ions distribute symmetrically with respect to that of the CF_2^+ ion. The most probable correlation angles between the momentum vectors of CF_2^+ and two F^+ ions are about the same (122° and 124°) indicating that the events in region B and region C come from the fragmentation of two distinct geometries of CF_4^{3+} . Figures 9(c), 9(f), and 9(i) show the KER distributions for regions A–C. The distinct KER peak values indicate that different excited states of CF_4^{3+} may be involved in these three processes.

With the help of the native frame method, the branching ratio of different mechanisms can be determined. For the

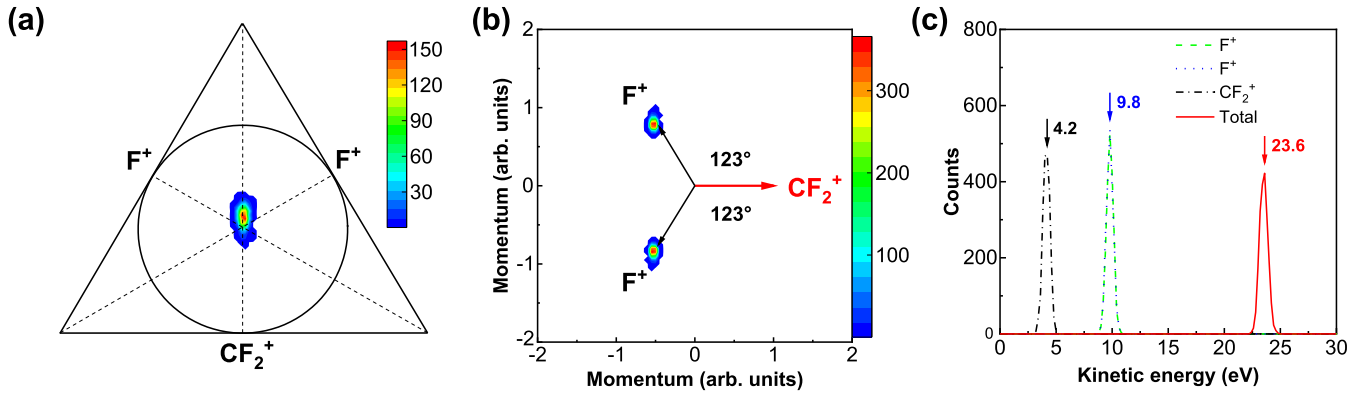


FIG. 10. Dalitz-like momentum diagram (a), Newton diagram (b), and KER distribution (c) obtained from the Coulomb explosion model simulation.

sequential fragmentation, we assume a uniform angular distribution from 0° to 180° in Fig. 8(c). Thereby, the total counts from sequential fragmentation can be determined by scaling the area of region A. Subtracting the counts of sequential fragmentation, the rest of the counts in region B together with region C are assigned to be the concerted mechanism. The branching ratio of the sequential breakup pathway and the concerted breakup pathways are estimated to be $17\% \pm 5\%$ and $83\% \pm 5\%$, respectively, where the uncertainty is determined by considering the standard derivation. The branching ratio of region C to the total counts is determined to be about $10\% \pm 1.5\%$.

Additionally, we employ the Coulomb explosion model to simulate the fragmentation process of CF_4^{3+} into $\text{F}^+ + \text{F}^+ + \text{CF}_2^+$. The assumptions in the simulation are as follows: (i) A vertical ionization from neutral to CF_4^{3+} is assumed. (ii) The fragments are driven by pure Coulomb repulsive forces between point charges placed at the center of mass of each fragment. (iii) The zero-point vibrational motion of the molecule is taken into consideration which is performed by a Wigner distribution.

In the end of the simulation, we extract the momentum vectors and kinetic energies of three fragment ions from which the simulated Dalitz-like momentum diagram, Newton diagram, and KER distribution are obtained. As shown in Fig. 10, the simulated results agree well with the experimental results of region C in Fig. 9. The small differences between the experimental and simulated Dalitz-like momentum diagram and Newton diagram may originate from contamination by the events of other fragmentation pathways due to the incomplete efficiency of the filter window in Fig. 8(c). Therefore, we propose that the events in region C of Fig. 8(c) are produced by fragmentation of CF_4^{3+} ions that have the same geometry as the neutral CF_4 molecule, while those events in region A and region B are created by CF_4^{3+} ions that have deformed geometries from the neutral CF_4 molecule.

IV. CONCLUSIONS

In summary, the fragmentation dynamics of CF_4^{q+} ($q = 2, 3$) induced by 1-keV electron impact is studied. From the

TOF correlation maps, a variety of fragmentation channels are observed. The KER distributions for these channels are obtained. Dalitz-like momentum diagrams and Newton diagrams are utilized to analyze the three-body fragmentation dynamics. For channels $\text{CF}_4^{2+} \rightarrow \text{F}^+ + \text{CF}_2^+ + \text{F}$ and $\text{F}^+ + \text{CF}^+ + 2\text{F}$, earlier works concluded sequential fragmentation mechanisms while a strong evidence for a concerted mechanism is found for these channels together with channel $\text{CF}_4^{2+} \rightarrow \text{F}^+ + \text{F}^+ + \text{CF}_2$ in this work. For the aforementioned channels, we found that the concerted mechanism is dominating the dissociation. On the other hand, the sequential mechanism is also not negligible if the neutral fragment is ejected in the first step. For channel $\text{CF}_4^{2+} \rightarrow \text{C}^+ + \text{F}^+ + 3\text{F}$, the initial charge separation is the dominating breakup process. One sequential and two concerted fragmentation processes are identified for channel $\text{CF}_4^{3+} \rightarrow \text{F}^+ + \text{F}^+ + \text{CF}_3^+$. The results show that the branching ratios of the concerted breakup pathways and the sequential breakup pathway are about $83\% \pm 5\%$ and $17\% \pm 5\%$, respectively. The distinct momentum correlations and KER distributions for these pathways indicate that different excited states of CF_4^{3+} with different geometries may be involved in the dissociation processes. The Coulomb explosion model simulations indicate that only a small number of the events in this channel are produced by CF_4^{3+} ions in the same geometry as the neutral CF_4 molecule while most of the events are created from deformed geometries.

ACKNOWLEDGMENTS

This work is supported by the National Key Research and Development Program of China (Grants No. 2017YFA0402300 and No. 2017YFA0303500), the Strategic Priority Research Program of the Chinese Academy of Sciences (Grant No. XDB34020000), the Fundamental Research Funds for the Central Universities (Grant No. WK2030000048), and the National Natural Science Foundation of China (Grants No. 11534011 and No. 11874339).

- [1] E. A. Müller, *Environ. Sci. Technol.* **39**, 8736 (2005).
- [2] P. Kowalczyk and R. Holyst, *Environ. Sci. Technol.* **42**, 2931 (2008).
- [3] P. Fabian and O. N. Singh, *Reactive Halogen Compounds in the Atmosphere* (Springer-Verlag, New York, 1999).
- [4] K. Denpoh and K. Nanbu, *J. Vac. Sci. Technol. A* **16**, 1201 (1998).
- [5] M. R. Bruce, C. Ma, and R. A. Bonham, *Chem. Phys. Lett.* **190**, 285 (1992).
- [6] L. Mi, C. R. Sporleder, and R. A. Bonham, *Chem. Phys. Lett.* **251**, 252 (1996).
- [7] M. R. Bruce, L. Mi, C. R. Sporleder, and R. A. Bonham, *J. Phys. B: At., Mol. Opt. Phys.* **27**, 5773 (1994).
- [8] D. M. Curtis and J. H. D. Eland, *Int. J. Mass Spectrom. Ion Process.* **63**, 241 (1985).
- [9] K. Codling, L. J. Frasinskit, P. A. Hatherlyt, M. Stankiewicz, and F. P. Larkins, *J. Phys. B: At., Mol. Opt. Phys.* **24**, 951 (1991).
- [10] N. Saito, J. D. Bozek, and I. H. Suzuki, *J. Phys. B: At., Mol. Opt. Phys.* **28**, 3505 (1995).
- [11] M. K. Thomas, B. O. Fisher, P. A. Hatherly, K. Codling, M. Stankiewicz, and M. Roper, *J. Phys. B: At., Mol. Opt. Phys.* **32**, 2611 (1999).
- [12] R. Feifel, J. H. D. Eland, L. Storchi, and F. Tarantelli, *J. Chem. Phys.* **125**, 194318 (2006).
- [13] N. Saito, J. D. Bozek, and I. H. Suzuki, *Chem. Phys.* **188**, 367 (1994).
- [14] K. Motohashi and S. Tsurubuchi, *J. Phys. B: At., Mol. Opt. Phys.* **36**, 1811 (2003).
- [15] O. Abu-Haija, S. A. Al-Faify, G. Olmez, S. M. Ferguson, and E. Y. Kamber, *Nucl. Instrum Methods Phys. Res., Sect. B* **241**, 109 (2005).
- [16] D. Wang, Y. Fan, Z. Zhao, G. Min, and X. Zhang, *J. Phys. B: At., Mol. Opt. Phys.* **49**, 165201 (2016).
- [17] J. H. D. Eland and B. J. Treves-Brown, in *Synchrotron Radiation and Dynamic Phenomena*, AIP Conf. Proc. No. 258 (AIP, Melville, NY, 1992), p. 100.
- [18] J. H. D. Eland, L. A. Coles, and H. Bountra, *Int. J. Mass Spectrom. Ion Processes* **89**, 265 (1989).
- [19] J. H. D. Eland, *Laser Chem.* **11**, 259 (1991).
- [20] N. Neumann, D. Hant, L. P. H. Schmidt, J. Titze, T. Jahnke, A. Czasch, M. S. Schöffler, K. Kreidi, O. Jagutzki, H. Schmidt-Böcking, and R. Dörner, *Phys. Rev. Lett.* **104**, 103201 (2010).
- [21] E. Wang, X. Shan, Z. Shen, M. Gong, Y. Tang, Y. Pan, K. C. Lau, and X. Chen, *Phys. Rev. A* **91**, 052711 (2015).
- [22] C. Wu, C. Wu, D. Song, H. Su, Y. Yang, Z. Wu, X. Liu, H. Liu, M. Li, Y. Deng, Y. Liu, L. Y. Peng, H. Jiang, and Q. Gong, *Phys. Rev. Lett.* **110**, 103601 (2013).
- [23] E. Wang, M. Gong, Z. Shen, X. Shan, X. Ren, A. Dorn, and X. Chen, *J. Chem. Phys.* **149**, 204301 (2018).
- [24] K. Lin, X. Hu, S. Pan, F. Chen, Q. Ji, W. Zhang, H. Li, J. Qiang, F. Sun, X. Gong, H. Li, P. Lu, J. Wang, Y. Wu, and J. Wu, *J. Phys. Chem. Lett.* **11**, 3129 (2020).
- [25] T. Jiang, B. Wang, Y. Zhang, L. Wei, S. Chen, W. Yu, Y. Zou, L. Chen, and B. Wei, *Phys. Rev. A* **100**, 022705 (2019).
- [26] S. Xu, X. L. Zhu, W. T. Feng, D. L. Guo, Q. Zhao, S. Yan, P. Zhang, D. M. Zhao, Y. Gao, S. F. Zhang, J. Yang, and X. Ma, *Phys. Rev. A* **97**, 062701 (2018).
- [27] C. Ma, S. Xu, D. Zhao, D. Guo, S. Yan, W. Feng, X. Zhu, and X. Ma, *Phys. Rev. A* **101**, 052701 (2020).
- [28] K. Ueda, M. Kitajima, A. De Fanis, T. Furuta, H. Shindo, H. Tanaka, K. Okada, R. Feifel, S. L. Sorensen, H. Yoshida, and Y. Senba, *Phys. Rev. Lett.* **90**, 233006 (2003).
- [29] R. Guillemin, W. C. Stolte, M. N. Piancastelli, and D. W. Lindle, *Phys. Rev. A* **82**, 043427 (2010).
- [30] Y. Pertot, C. Schmidt, M. Matthews, A. Chauvet, M. Huppert, V. Svoboda, A. von Conta, A. Tehlar, D. Baykusheva, J.-P. Wolf, and H. J. Wörner, *Science* **355**, 264 (2017).
- [31] Y. Hikosaka and E. Shigemasa, *J. Electron Spectrosc. Relat. Phenom.* **152**, 29 (2006).
- [32] K. A. Larsen, C. S. Trevisan, R. R. Lucchese, S. Heck, W. Iskandar, E. Champenois, A. Gatton, R. Moshhammer, R. Strom, T. Severt, B. Jochim, D. Reedy, M. Weller, A. L. Landers, J. B. Williams, I. Ben-Itzhak, R. Dörner, D. Slaughter, C. W. McCurdy, T. Weber *et al.*, *Phys. Chem. Chem. Phys.* **20**, 21075 (2018).
- [33] X. Tang, X. Zhou, M. Wu, Z. Gao, S. Liu, F. Liu, X. Shan, and L. Sheng, *J. Chem. Phys.* **138**, 094306 (2013).
- [34] H. Fukuzawa, X. J. Liu, T. Teranishi, K. Sakai, G. Prümper, K. Ueda, Y. Morishita, N. Saito, M. Stener, and P. Decleva, *Chem. Phys. Lett.* **451**, 182 (2008).
- [35] S. E. Sobottka and M. B. Williams, *IEEE Trans. Nucl. Sci.* **35**, 348 (1988).
- [36] O. Jagutzki, V. Mergel, K. Ullmann-Pfleger, L. Spielberger, U. Spillmann, R. Dörner, and H. Schmidt-Böcking, *Nucl. Instrum. Methods Phys. Res., Sect. A* **477**, 244 (2002).
- [37] R. Dörner, V. Mergel, O. Jagutzki, L. Spielberger, J. Ullrich, R. Moshhammer, and H. Schmidt-Böcking, *Phys. Rep.* **330**, 95 (2000).
- [38] J. Ullrich, R. Moshhammer, A. Dorn, R. Dörner, L. P. H. Schmidt, and H. Schmidt-Böcking, *Rep. Prog. Phys.* **66**, 1463 (2003).
- [39] R. H. Dalitz, *London, Edinburgh Dublin Philos. Mag. J. Sci.* **44**, 1068 (1953).
- [40] J. Rajput, T. Severt, B. Berry, B. Jochim, P. Feizollah, B. Kaderiya, M. Zohrabi, U. Ablikim, F. Ziaee, K. Raju P., D. Rolles, A. Rudenko, K. D. Carnes, B. D. Esry, and I. Ben-Itzhak, *Phys. Rev. Lett.* **120**, 103001 (2018).
- [41] L. Chen, X. Shan, E. Wang, X. Ren, X. Zhao, W. Huang, and X. Chen, *Phys. Rev. A* **100**, 062707 (2019).
- [42] W. C. Wiley and I. H. McLaren, *Rev. Sci. Instrum.* **26**, 1150 (1955).
- [43] I. Torres, R. Martínez, and F. Castaño, *J. Phys. B: At., Mol. Opt. Phys.* **35**, 2423 (2002).
- [44] H. Iwayama, C. Léonard, F. Le Quéré, S. Carniato, R. Guillemin, M. Simon, M. N. Piancastelli, and E. Shigemasa, *Phys. Rev. Lett.* **119**, 203203 (2017).
- [45] F. P. Larkins and L. C. Tulea, *J. Phys. Colloq.* **48**, C9-725 (1987).
- [46] W. J. Griffiths, S. Svensson, A. Naves de Brito, N. Correia, C. J. Reid, M. L. Langford, F. M. Harris, C. M. Liegener, and H. Ågren, *Chem. Phys.* **173**, 109 (1993).
- [47] F. O. Gottfried, L. S. Cederbaum, and F. Tarantelli, *J. Chem. Phys.* **104**, 9754 (1996).
- [48] H. M. Rosenstock, K. Draxl, B. W. Steiner, and J. T. Herron, *J. Phys. Chem. Ref. Data* **6**(Suppl. 1), I-83 and I-350 (1977).
- [49] A. Matsuda, E. J. Takahashi, and A. Hishikawa, *J. Chem. Phys.* **127**, 114318 (2007).